Global gyrokinetic multi-model simulations of ITG and Alfvénic modes for tokamaks and the first operational phase of Wendelstein 7-X

R. Kleiber, M. Borchardt, A. Könies, A. Mishchenko, J. Riemann, C. Slaby
Max-Planck-Institut für Plasmaphysik, 17491 Greifswald, Germany

R. Hatzky
Max-Planck-Institut für Plasmaphysik, 85748 Garching, Germany

Email: ralf.kleiber@ipp.mpg.de

Abstract

Several results from applying the global gyrokinetic particle-in-cell code EUTERPE to tokamak and stellarator configurations are presented. Linear low-mode-number AITG modes were simulated for an LHD-like equilibrium. Using a Fourier solver approach, long-time fully kinetic runs of damped TAEs could be performed. Super-resolution methods allowed us to accurately resolve the continuous Alfvén spectrum.

Results from a hybrid approach (CKA-EUTERPE code), which couples an MHD code with a gyrokinetic code are presented. Although perturbative, it offers a relatively fast way to investigate the destabilisation of Alfvén modes by fast particles. TAE saturation amplitudes and their scaling with collisionality were investigated in a tokamak as well as in Wendelstein 7-X. Also frequency chirping in the non-linear phase of the simulation could be observed.

Linear electrostatic gyrokinetic simulations for Wendelstein 7-X and an LHD-like configuration show the influence of a radial neoclassical electric field on the ITG growth rate.

In the interest of the next operational phase, geodesic acoustic mode oscillations were investigated for Wendelstein 7-X.

1 Introduction

Fully electromagnetic gyrokinetic simulations usually require long computing times. For identifying interesting regimes it is thus necessary to develop physically reduced models which allow for much faster computations. This approach was implemented into the global gyrokinetic particle-in-cell code EUTERPE. Figure 1 shows the hierarchy of models [1] used. It ranges from a complex fully gyrokinetic model, fluid model [2] up to a relatively simple MHD hybrid model.
In the following, we will present recent results from two of those models: EUTERPE and CKA-EUTERPE.

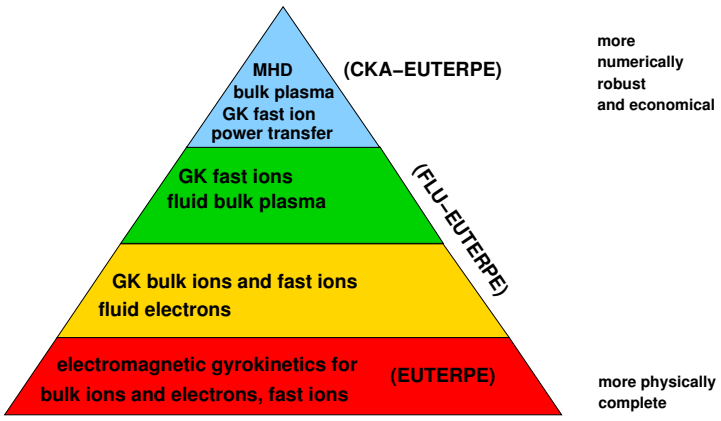

Figure 1: Hierarchy of models implemented in EUTERPE.

2 Equations

Two different physical models will be used in the following: The gyrokinetic model, which is physically comprehensive but requires very long simulation times, and a non-linear MHD-gyrokinetic hybrid model (CKA-EUTERPE) which is only perturbative but very fast and numerically stable.

2.1 Gyrokinetic model

Employing the formalism of gyrokinetic field theory [3] the model can be concisely defined by the Lagrangian in the phase space $\{\vec{R}, p_\parallel, \mu, \alpha\}$:

$$\begin{aligned} L = \sum_{\text{species}} \int \Bigg\{ f \left[(q\vec{A} + m v_\parallel \vec{b}) \cdot \dot{\vec{R}} + \frac{m^2}{q} \mu \dot{\alpha} - \frac{m}{2} v_\parallel^2 - m\mu B - q\langle\phi\rangle + q v_\parallel \langle A_\parallel \rangle \right] + \\ f_0 \left[\frac{m}{2B^2} (\nabla_\perp \phi)^2 - \frac{q^2}{2m} \langle A_\parallel \rangle^2 \right] \Bigg\} \mathrm{d}V \mathrm{d}W - \frac{1}{2\mu_0} \int (\nabla_\perp A_\parallel)^2 \mathrm{d}V \end{aligned} \tag{1}$$

Here $\vec{R}$ is the guiding centre position and $\{p_\parallel, \mu, \alpha\}$ are the canonical parallel momentum, magnetic moment and gyro angle, respectively. The volume elements are given by $\mathrm{d}W = B_\parallel^* \, \mathrm{d}p_\parallel \, \mathrm{d}\mu \, \mathrm{d}\alpha$ and $\mathrm{d}V = \sqrt{g} \, \mathrm{d}s \, \mathrm{d}\vartheta \, d\varphi$ (with $\sqrt{g}$ the Jacobian and $B_\parallel^* = B + \frac{1}{q} p_\parallel \vec{b} \cdot \nabla \times \vec{b}$). The distribution function and the Maxwellian are denoted by f and f_0, respectively. The quantities q and m are the charge and mass of the corresponding species, $\langle \cdot \rangle$ is the gyroaveraging operator, and $\vec{A}$ and $\vec{b}$ are the vector potential and the unit field vector of the background magnetic field. The dynamical variables are the electrostatic potential ϕ and the parallel vector potential $A_\parallel$. A long wavelength approximation has been employed in the field energy term for ϕ (for arbitrary wavelength simulations, a Padé approximation is available). Furthermore, it is assumed that $\nabla_\perp$ and $\langle \cdot \rangle$ act only in the poloidal plane.

2.2 Hybrid model

For the hybrid model the electrostatic potential (and similarly the parallel vector potential) is assumed to have the form

$$\phi = \mathrm{Re}[\hat{\phi}(t) \, \phi_0 \exp(\mathrm{i}\omega t)]. \tag{2}$$

Here, the eigenmode ϕ_0 and its frequency ω is obtained by the reduced ideal MHD code CKA [4]. Assuming a scale separation between ω and the time evolution of the mode amplitudes, the latter one develop as

$$\frac{\partial \hat{\phi}(t)}{\partial t} = \mathrm{i}\omega \left(\hat{A}_\parallel - \hat{\phi} \right) + 2 \left(\gamma(t) - \gamma_\mathrm{d} \right) \hat{\phi} \tag{3}$$

$$\frac{\partial \hat{A}_\parallel(t)}{\partial t} = \mathrm{i}\omega \left(\hat{\phi} - \hat{A}_\parallel \right). \tag{4}$$

The ad-hoc damping rate γ_d can be used to mimic effects not covered by the MHD model (e.g. continuum and Landau damping). The time dependent growth rate 2γ is given by the ratio of the wave-particle energy transfer, which is calculated by solving the gyrokinetic equation, and the mode energy. For non-linear simulations the real parts of ϕ and $A_\parallel$ multiplied by a phase factor determine the trajectories of the particles.

3 Results

Two recently developed numerical methods, the pullback transformation scheme [5] and the Fourier solver [6], allow robust electromagnetic simulations of large scale modes over long times. Especially the simulation of stable modes is a serious test for the quality of the numerical algorithms.

3.1 Alfvénic ITG mode in a stellarator

Figure 2 shows the simulation result of a low wave number AITG mode (dominant $m \approx 7$) in an LHD variant. For the fast particles a constant density of $1{\cdot}10^{18}\mathrm{m}^3$ and an energy of 70 keV has been assumed. The mode is destabilised by the gradients of the bulk plasma. Increasing the constant electron density n_e from $1{\cdot}10^{19}$ m^{-3} to $6{\cdot}10^{19}$ m^{-3} leads to a fourfold increase of the growth rate. Comparing to the case without fast particles one finds that they act slightly stabilising.

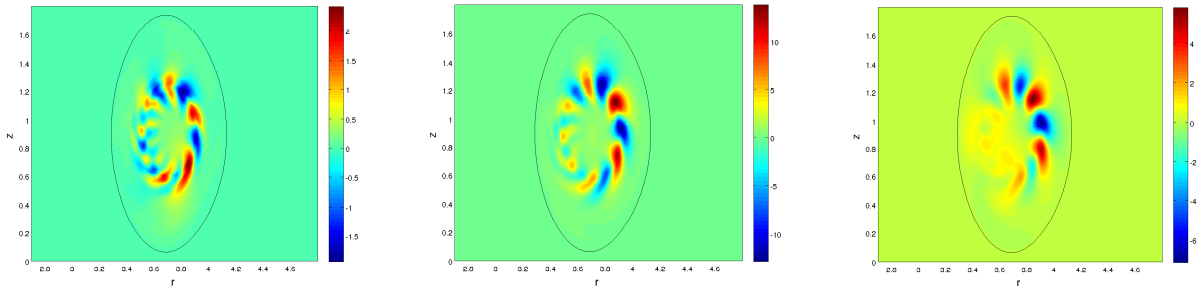

Figure 2: Electrostatic potential in a poloidal cross section at $\phi = 0$. Left to right: electron density $n_\mathrm{e} = (1, 2, 6){\cdot}10^{19}$ m^{-3}

.

3.2 Stable TAE modes in a tokamak

Here, a circular tokamak equilibrium with aspect ratio $A = 10$ (ITPA benchmark case [7, 8]) was used. Starting the simulation from noise, one gets a mixture of damped Alfvén modes. Employing super-resolution spectral estimation methods it is possible to obtain a radially resolved frequency spectrum where the Alfvén continua are clearly visible (see Figure 3). At the continuum gaps, around $s = 0.25$ and $s = 0.8$, TAE modes are observed. Also a GAM up-shift of the lowest frequency branch around $s = 0.8$ is visible. For ideal MHD modes, the positive and negative frequency part of the spectrum are identical. In the simulation result shown here, this degeneracy in $|\Omega|$ is slightly lifted by kinetic effects. In order to resolve this phenomenon, the simulation was initialised with a smooth perturbation instead of noise. Figure 4 (left) shows a cut along $s = 0.25$ through the lowest frequency part of the spectrum, i.e. the TAE mode, as a function of $|\Omega|$. The difference in frequency between the negative and positive frequency mode is below 1 %. The kinetic damping of the two modes is quite different: the positive frequency mode is damped 3.6 times more strongly than the negative frequency mode. The damping rate is very small, less than 0.4% of the frequency, which makes its determination prone to numerical inaccuracies. The tiny difference in frequency is an additional reason why it is so difficult to accurately simulate damped TAE: During a simulation the weakest damped mode should win against the other modes after some time. The slightly different frequencies induce a beating which on short times may lead one to believe that the damping rate is stronger. Therefore, very long runs are necessary for obtaining a precise value of the damping rate [9] (see Figure 4, right).

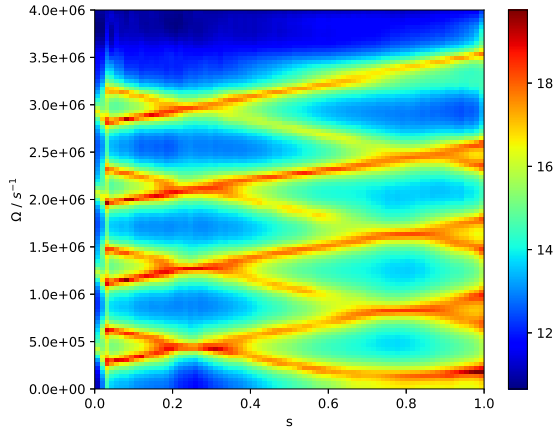

Figure 3: Frequency spectrum as a function of the flux surface label s.

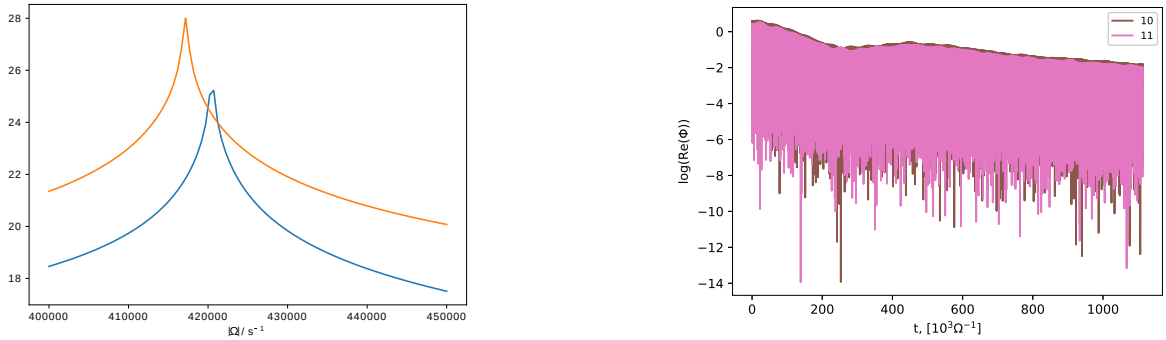

Figure 4: Left: Frequency spectrum as a function of $|\Omega|$. Blue/orange colour signifies the positive/negative frequency branch. The corresponding damping rates are $440\,\mathrm{s}^{-1}$ and $1600\,\mathrm{s}^{-1}$. Right: Time trace of the $m = 10, 11$ Fourier component of $\mathrm{Re}(\phi)$ (about 250 oscillation periods are shown).

3.3 Collisional scaling of the saturation level of a TAE in Wendelstein 7-X

With the CKA-EUTERPE code, TAE saturation amplitudes and their scaling with growth rate were investigated in a tokamak as well as in Wendelstein 7-X (W7-X) using non-linear simulations.
Recently, pitch-angle collisions have been implemented and benchmarked for the electromagnetic version of EUTERPE [10]. This initial benchmark was done in slab geometry. A more rigorous comparison to analytic theory is possible in the framework of the well-known Berk-Breizman model [11]. For the case of a TAE mode influenced by pitch-angle collisions it predicts a $\nu^{\frac{2}{3}}$ scaling of the saturation amplitudes with collision frequency ν. The first maximum after the linear phase here is referred to as the saturation amplitude. In a tokamak, the predicted scaling is confirmed numerically for low-enough collision frequencies in the resonance detuning regime [12].
However, in the W7-X scenario studied here a different scaling was found (see Figure 5). For low collision frequencies the saturation level scales only with $\nu^{0.28}$ [13]. For high collision frequencies, pitch-angle collisions even reduce the saturation amplitude such that an overall non-monotonic scaling results. In spite of a strong variation in ν, the saturation amplitude changes very little. A flattening of the fast ions density profile by TAE-induced transport was also observed [13].

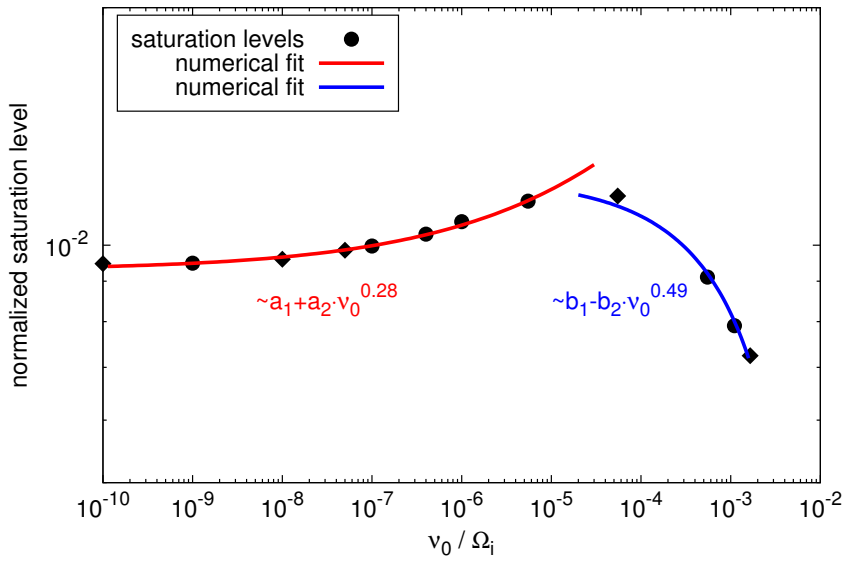

Figure 5: Scaling of the saturation level of the poloidal magnetic field perturbation with the collision frequency for a Wendelstein 7-X high-mirror case.

3.3.1 Frequency chirping of Alfvén eigenmodes

In a tokamak it was found that, depending on the linear growth rate of the mode, the saturation dynamics is altered from a symmetric chirping for small growth rates over an asymmetric chirping regime to a decaying mode [14].
During the 2018 experimental campaign of W7-X, neutral beam injection (providing fast ions) became available. In order to develop our tools towards comparison with experimental results the frequency chirping of a fast-ion-driven TAE was simulated for a W7-X high-mirror configuration [14]. This configuration was chosen because it shows the best fast ion confinement [15]. The simulations include a slowing-down distribution function for the fast ions. It was obtained by fitting results from the ASCOT code [16] to the model implemented in EUTERPE. Figure 6 shows time-frequency distributions of time traces of ϕ in the non-linear regime generated using the S-method. The left-hand side shows multiple chirping events. Periodic chirping of Alfvén eigenmodes is observed in many devices [17, 18]. In the present case, periodic chirping is achieved in the simulations by using a Krook operator as a simple proxy for a particle source. Consequently, the result (Figure 6, right) shows multiple periodic bursts of chirping. Berk-Breizman theory predicts that the linear growth rate, damping rate and collision frequencies are important parameters determining the shape of the chirping parabola [19]. Future simulations could provide guidance to determine e. g. the damping rate of experimentally observed modes, a quantity very difficult to measure directly.

3.4 Effects of a radial electric field on the electrostatic linear ITG instability in stellarators

The presence of a neoclassical radial electric field - constant on flux surfaces and necessary to fulfil the ambipolarity condition - is an important feature of stellarators. Depending on the operational regime, this field either points inward (so-called ion-root regime) or outwards (electron-root regime). With both cases being of interest, the ion-root regime appears as the most prevalent in experiments and was therefore considered via an electric field model $E_s \sim \frac{1}{n}\frac{\mathrm{d}p}{\mathrm{d}s}$ [20] in a series of linear ITG simulations.

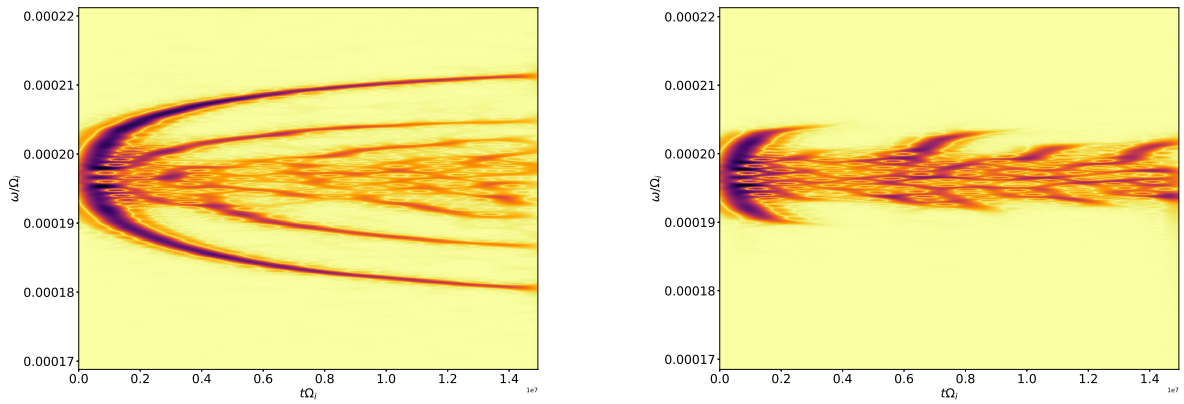

Figure 6: Left: Frequency chirping of a TAE in a Wendelstein 7-X high-mirror configuration without Krook operator. Right: Inclusions of a Krook operator (emulating a particle source) leads to periodic chirping events

These simulations were designed to supplement earlier studies (e.g. stability diagrams) of linear ITG properties in both W7-X and an LHD-like configuration. The focus was set on the impact of radial electric fields on linear ITG growth rates. The analysis of ITG mode frequencies, power spectra, spatial structure and localization – all being modified under the influence of the radial electric field – helped to explain the observed growth rates as the result of competing stabilizing mechanisms. The results in Figure 7 (here the Mach number is defined as $M = \langle |E \times B| \rangle / v_{\mathrm{th}}|_{s=0.5}$, with $\langle \cdot \rangle$ being the flux surface average) generally support the common view that radial electric fields may lead to a reduction of ITG instability growth. These fields give rise to an $E \times B$-drift which can lead to a spatial displacement of ITG mode structures and a simultaneous modification of characteristic mode properties. Due to their different geometric properties, W7-X and LHD were seen to lead to qualitatively different ITG modes. Different stabilizing mechanisms - the influence of a (mainly) poloidal drift of ITG mode structures as well as the action of mode shearing - can be recognized for both W7-X and LHD. Those mechanisms seem to play a more or less dominant role, depending on the configuration and the strength of the radial electric fields. For W7-X with its pronounced helical edge on the outboard side at the plasma boundary, the distortion of ITG modes due to the variation of metric properties seems to be dominant. For LHD with its smoothly varying curvature on the outboard side of the torus, the spatial displacement of ITG modes into regions with reduced instability growth can explain the observed reduction of growth rates well [21].

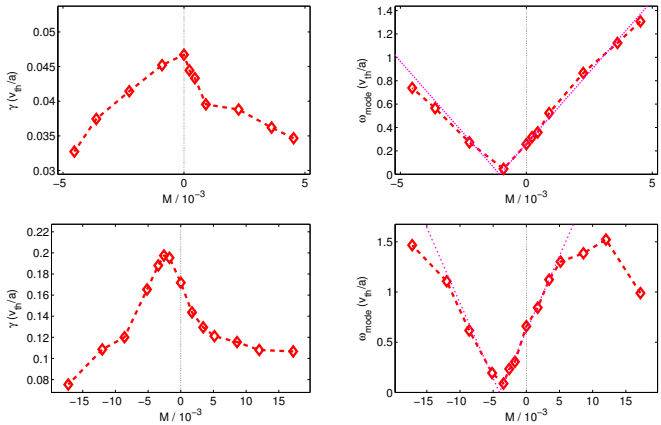

Figure 7: Growth rates (left) and mode frequencies (right) for W7-X (top) and LHD (bottom) vs. $E \times B$-Mach numbers from radial electric fields according to the model by Ehmler et al., derived for the ion-root regime. Flat density $a/L_n = 0$ together with $a/L_T = 1.41$ (Wendelstein 7-X) and $a/L_T = 4.23$ (LHD) were assumed. Magenta curves correspond to frequencies derived from a Doppler-shift model.

3.5 Simulation of geodesic acoustic modes in W7-X

In the low-ι OP 1.2 (the second major operating phase) W7-X configuration (with a central ι of about 0.75) GAMs are strongly damped. After a short time, only the low frequency zonal flow oscillations [22, 23] remain (see Figure 8, left). Since the GAM damping rate scales as $\gamma_{\mathrm{GAM}} \sim \exp\left(-\frac{R^2\omega_{\mathrm{GAM}}^2}{\iota^2 v_{T_\mathrm{i}}^2}\right)$, with $\omega_{\mathrm{GAM}}^2 \approx \frac{v_{T_\mathrm{i}}^2}{R^2}\left(\frac{7}{4}+\frac{T_\mathrm{e}}{T_\mathrm{i}}\right)$, one would expect weakly-damped GAMs if ι was reduced. Figure 8 (right) shows the result for an equilibrium where a plasma current (e.g. by ECCD) was used to reduce the central ι to a value of 0.2. Now GAMs which are weakly damped for $s < 0.5$ can be observed in the simulations. This may offer the possibility of finding GAMs in W7-X for experiments with suitable modified equilibria.

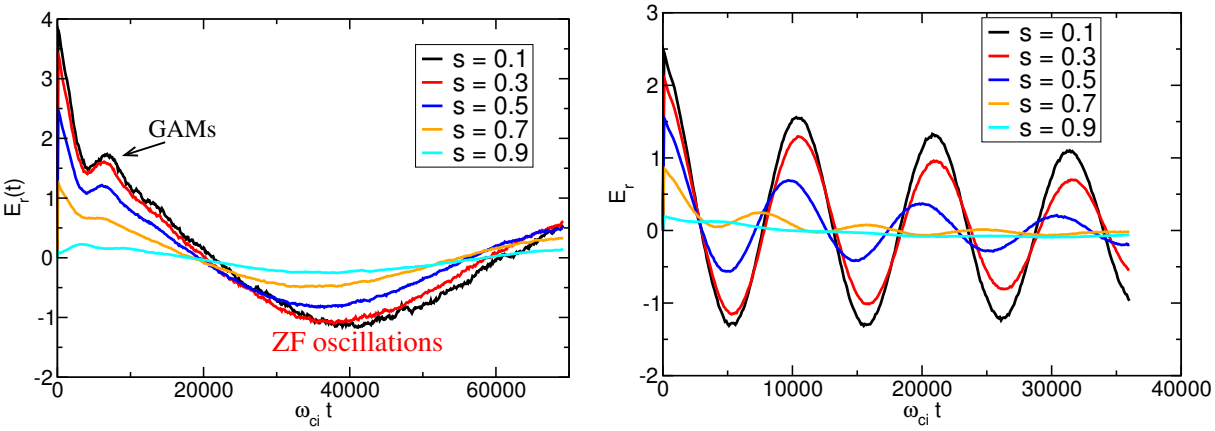

Figure 8: Zonal flow radial electric field at different flux surfaces for W7-X. Left: low-ι OP 1.2 equilibrium where GAMs are quickly damped, Right: equilibrium where ι has been strongly reduced by a plasma current and GAMs can be seen for lower s.

Acknowledgements

This work has been carried out within the framework of the EUROfusion Consortium and has received funding from the Euratom research and training programme 2014-2018 under grant agreement No 633053. The views and opinions expressed herein do not necessarily reflect those of the European Commission.

References

[1] M. Cole, A. Mishchenko, A. Könies, R. Hatzky, R. Kleiber, A hierarchy of electromagnetic gyrokinetic and fluid hybrid models for the simulation of global modes, Plasma Phys. Controlled Fusion 57 (2015) 054013.

[2] M. Cole, A. Mishchenko, A. Könies, R. Kleiber, M. Borchardt, Fluid electron, gyrokinetic ion simulations of linear internal kink and energetic particle modes, Phys. Plasmas 21 (2014) 072123.

[3] B. Scott, J. Smirnov, Energetic consistency and momentum conservation in the gyrokinetic description of tokamak plasmas, Phys. Plasmas 17 (2010) 112302.

[4] T. Feher, Nonlinear gyrokinetic equations for low-frequency electromagnetic waves in general plasma equilibria, Ph.D. thesis, 2013.

[5] A. Mishchenko, A. Könies, R. Kleiber, M. Cole, Pullback transformation in gyrokinetic electromagnetic simulations, Phys. Plasmas 21 (2014) 092110.

[6] M. Borchardt et al., in preparation.

[7] A. Könies, S. Briguglio, N. Gorelenkov, T. Fehér, M. Isaev, P. Lauber, A. Mishchenko, D. A. Spong, Y. Todo, W. A. Cooper, R. Hatzky, R. Kleiber, M. Borchardt, G. Vlad, ITPA EP TG, Benchmark of gyrokinetic, kinetic mhd and gyrofluid codes for the linear calculation of fast particle driven TAE dynamics, IAEA-FEC (2012) ITR/P1–34.

[8] A. Könies, S. Briguglio, N. Gorelenkov, T. Fehér, M. Isaev, P. Lauber, A. Mishchenko, D. A. Spong, Y. Todo, W. A. Cooper, R. Hatzky, R. Kleiber, M. Borchardt, G. Vlad, ITPA EP TG, Benchmark of gyrokinetic, kinetic MHD and gyrofluid codes for the linear calculation of fast particle driven TAE dynamics, accepted at Nuclear Fusion.

[9] A. Könies et al., in preparation.

[10] C. Slaby, R. Kleiber, A. Könies, Combining electromagnetic gyro–kinetic particle–in–cell simulations with collisions, Comp. Phys. Commun. 218 (2017) 1.

[11] H. L. Berk, B. N. Breizman, H. Ye, Scenarios for the nonlinear evolution of alpha-particle-induced Alfvén wave instability, Phys. Rev. Lett. 68 (1992) 3563.

[12] S. Briguglio, X. Wang, F. Zonca, G. Vlad, G. Fogaccia, C. Di Troia, V. Fusco, Analysis of the nonlinear behavior of shear-Alfvén modes in tokamaks based on hamiltonian mapping techniques, Phys. Plasmas 21 (2014) 112301.

[13] C. Slaby, A. Könies, R. Kleiber, José Manuel Garcia-Regaña, Effects of collisions on the saturation dynamics of TAEs in tokamaks and stellarators, Nucl. Fusion 58 (2018) 082018.

[14] C. Slaby et al., submitted to nuclear fusion.

[15] S. Äkäslompolo, M. Drevlak, Y. Turkin, S. Bozhenkov, T. Jesche, J. Kontula, T. Kurki-Suonio, R. C. Wolf, the W7-X Team, Modelling of NBI ion wall loads in the W7-X stellarator, Nucl. Fusion 58 (2018) 082010.

[16] E. Hirvijoki, O. Asunta, T. Koskela, T. Kurki-Suonio, J. Miettunen, S. Sipilä, A. Snicker, S. Äkäslompolo, ASCOT: Solving the kinetic equation of minority particle species in tokamak plasmas, Comp. Phys. Commun. 185 (2014) 1310.

[17] M. García-Muñoz, N. Hicks, R. van Voornveld, I. G. J. Classen, R. Bilato, V. Bobkov, M. Bruedgam, H.-U. Fahrbach, V. Igochine, S. Jaemsae, M. Maraschek, K. Sassenberg, Convective and diffusive energetic particle losses induced by shear Alfvén waves in the ASDEX upgrade tokamak, Phys. Rev. Lett. 104 (2010) 185002.

[18] A. Melnikov, L. Eliseev, E. Ascasbar, A. Cappa, F. Castejn, C. Hidalgo, T. Ido, J. Jimnez, A. Kozachek, L. Krupnik, M. Liniers, S. Lysenko, K. Nagaoka, J. de Pablos, A. Shimizu, S. Sharapov, M. Ufimtsev, S. Yamamoto, HIBP group, TJ-II team, Transition from chirping to steady NBI-driven Alfvén modes caused by magnetic configuration variations in the TJ-II stellarator, Nucl. Fusion 56 (2016) 076001.

[19] M. Lesur, Y. Idomura, K. Shinohara, X. Garbet, Spectroscopic determination of kinetic parameters for frequency sweeping alfvén eigenmodes, Phys. Plasmas 17 (2010) 122311.

[20] H. Ehmler, Y. Turkin, C. D. Beidler, H. Maassberg, A. Dinklage, T. Klinger, W.-A. Team, Experimental check of neoclassical predictions for the radial electric field in a stellarator, Nucl. Fusion 43 (2003) L11.

[21] J. Riemann, R. Kleiber, M. Borchardt, Effects of radial electric fields on linear ITG instabilities in W7-X and LHD, Plasma Phys. Controlled Fusion 58 (2016) 074001.

[22] P. Helander, A. Mishchenko, R. Kleiber, P. Xanthopoulos, Oscillations of zonal flows in stellarators, Plasma Phys. Controlled Fusion 53 (2011) 054006.

[23] A. Mishchenko, R. Kleiber, Zonal flows in stellarators in an ambient radial electric field, Phys. Plasmas 19 (2012) 072316.